Med Biol Eng Comput (2015) 53:815–828
DOI 10.1007/s11517-015-1276-9

ORIGINAL ARTICLE

Upper-limb kinematic reconstruction during stroke robot-aided therapy

E. Papaleo[1] · L. Zollo[1] · N. Garcia-Aracil[2] · F. J. Badesa[2] · R. Morales[2] · S. Mazzoleni[3] · S. Sterzi[4] · E. Guglielmelli[1]

Received: 30 November 2013 / Accepted: 7 March 2015 / Published online: 11 April 2015

Abstract The paper proposes a novel method for an accurate and unobtrusive reconstruction of the upper-limb kinematics of stroke patients during robot-aided rehabilitation tasks with end-effector machines. The method is based on a robust analytic procedure for inverse kinematics that simply uses, in addition to hand pose data provided by the robot, upper arm acceleration measurements for computing a constraint on elbow position; it is exploited for task space augmentation. The proposed method can enable in-depth comprehension of planning strategy of stroke patients in the joint space and, consequently, allow developing therapies tailored for their residual motor capabilities. The experimental validation has a twofold purpose: (1) a comparative analysis with an optoelectronic motion capturing system is used to assess the method capability to reconstruct joint motion; (2) the application of the method to healthy and stroke subjects during circle-drawing tasks with InMotion2 robot is used to evaluate its efficacy in discriminating stroke from healthy behavior. The experimental results have shown that arm angles are reconstructed with a RMSE of 8.3×10^{-3} rad. Moreover, the comparison between healthy and stroke subjects has revealed different features in the joint space in terms of mean values and standard deviations, which also allow assessing inter- and intra-subject variability. The findings of this study contribute to the investigation of motor performance in the joint space and Cartesian space of stroke patients undergoing robot-aided therapy, thus allowing: (1) evaluating the outcomes of the therapeutic approach, (2) re-planning the robotic treatment based on patient needs, and (3) understanding pathology-related motor strategies.

Keywords Upper-limb kinematics · Rehabilitation robotics · Stroke rehabilitation

✉ E. Papaleo
eugeniapapaleo@gmail.com; e.papaleo@unicampus.it
URL: http://www.biorobotics.it

L. Zollo
l.zollo@unicampus.it
URL: http://www.biorobotics.it

N. Garcia-Aracil
nicolas.garcia@umh.es
URL: http://www.nbio.umh.es

F. J. Badesa
fbadesa@umh.es
URL: http://www.nbio.umh.es

R. Morales
rmorales@umh.es
URL: http://www.nbio.umh.es

S. Mazzoleni
s.mazzoleni@sssup.it
URL: http://www.sssa.bioroboticsinstitute.it

S. Sterzi
s.sterzi@unicampus.it
URL: http://www.policlinicocampusbiomedico.it

E. Guglielmelli
e.guglielmelli@unicampus.it
URL: http://www.biorobotics.it

[1] Laboratory of Biomedical Robotics and Biomicrosystems, Università Campus Bio-Medico di Roma, Rome, Italy

[2] Virtual Reality and Robotics Lab, Universidad Miguel Hernandez de Elche, Elche, Spain

[3] BioRobotics Institute, Scuola Superiore Sant'Anna Pisa, Pisa, Italy

[4] Operative Unit of Physical Medicine and Rehabilitation, Università Campus Bio-Medico di Roma, Rome, Italy

1 Introduction

In Italy, about 200,000 persons are affected by stroke each year, and in USA approximately 795,000 Americans experience a new or recurrent stroke each year [12]. Most people survive, but the functionalities of the upper limb are often compromised [27]. Motor rehabilitation is proved to be very effective in dealing with upper-limb motor impairment resulting from stroke. In particular, the beneficial effects of *robot-aided therapy* and *constrained-induced movement therapy* were shown by several studies in the last decade [16].

Rehabilitation machines can be categorized into two main classes [13]: (1) exoskeletal robots and (2) end-effector robots, where the physical contact with the patient is limited to the end-effector. For historical reasons and for the reduced design complexity, end-effector machines are more commonly used in the clinical practice than exoskeletons [20, 22], with the consequent limitation that patient motion can be assessed only in the Cartesian space through the sensors embedded in the robot [3, 5, 6, 28], and patient joint motion cannot be directly monitored.

Nevertheless, the analysis of arm joint trajectories of stroke patients undergoing robot-aided therapy can address a number of scientific and clinical issues, such as:

- Quantifying the residual motor capabilities of the patient, by investigating the behavior of each degree of freedom involved in the motion.
- Assessing the outcomes of the therapy at Cartesian and joint level and, possibly, understanding the motor strategies possibly related to the pathology.
- Re-planning/re-configuring the treatment based on the recovery level and the motion capabilities of each specific patient.
- Improving patient safety keeping away arm motion from human joint limits.

- Typical systems for motion analysis (also used in clinics) are as follows: (1) electrogoniometers, (2) inertial or magneto-inertial sensors and (3) optoelectronic systems [2]. As regards electrogoniometers, it is difficult to eliminate the misalignment between the measuring system and the human joint axes of rotation; they are obtrusive systems and cannot measure rotations around the longitudinal axis of a limb segment (such as the shoulder intra-extra rotation). Inertial and magneto-inertial wearable sensors are cheap and small (due to the microfabrication procedures) and consume very low power [25]; however, they can be obtrusive and alter the natural motion of a subject if a net of sensors is used to reconstruct the entire arm kinematics. Optoelectronic devices are camera-based systems considered as the most accurate motion capturing systems as long as marker-based approaches are employed. However, they are very expensive and require a high structured acquisition environment and a time-consuming calibration procedure.

An alternative approach to the use of motion analysis systems relies on the use of computational methods to reconstruct upper-limb kinematics. In a recent review [10], it was stated that the most appropriate way to solve the upper-limb inverse kinematics problem is to resort to methodologies derived from robotics. Unless one considers a simplified planar human arm model, as in [8], the inverse kinematics approach requires to face the redundancy of the human arm kinematic chain. In [10], two general approaches to solve arm redundancy are proposed, both based on intrinsic kinematic constraints: (1) In the first approach, the minimization of the path covered from an initial to a final position is accounted for; (2) in the second one, underlying relations between joint angles are taken into account. However, while the first constraint has shown inconsistencies with the experimental observations, methods based on the second constraint were found valid only for particular movements, since the arm posture at a given hand position cannot be considered independent on previous configurations [31]. This is the case, for example, of the adaptation of the Donder's law to the human arm.

Other computational approaches for solving the upper-limb redundancy problem adopt simpler kinematic constraints or some geometrical simplifications [1]. The consequence is that estimations (and not accurate measures) of the upper-limb angles can be provided.

The objective of this paper is to propose a new approach that allows overcoming the shortcomings of the aforementioned systems and methods, and enables an accurate and unobtrusive reconstruction of the entire upper-limb kinematics in robot-aided rehabilitation with end-effector machines. The approach is based on an inverse kinematics algorithm, originally conceived for redundant anthropomorphic manipulators and here ad hoc adapted to human motion reconstruction. Hence, the method has the advantage to be grounded on a robust analytic procedure. The kinematic redundancy of the arm is solved through the task space augmentation; this allows obtaining a closed-form solution for the inverse kinematics problem. Constrained solutions are found by simply performing an additional measurement with respect to the hand pose data provided by the robot, i.e., the radial acceleration of the upper arm segment. In this way, the so-called *swivel angle* [14, 17] is computed (i.e., the angle that describes the internal motion of the upper-limb when shoulder and hand position are fixed), thus enabling parametrization of arm redundancy.

The kinematic model of the upper-limb and the inverse kinematics algorithm are presented in Sects. 2.1 and 2.2, respectively; the experimental tests carried out for assessing

the proposed method and measuring its performance are illustrated in Sect. 2.3. The experimental tests were carried out with a two-stage procedure: first, a comparative analysis with data measured by an optoelectronic marker-based digital system (SMART-D, from BTS Bioengineering) was performed; secondly, the method was applied to healthy and stroke subjects during the execution of circle-drawing tasks with the InMotion2 rehabilitation robot. Experimental results and discussion are reported in Sects. 3 and 4, respectively.

2 Methods

This section presents the upper-limb kinematic model, the theoretical formulation of the joint reconstruction algorithm and the two-stage procedure followed for validating the proposed method on healthy and pathological subjects.

2.1 Upper-limb kinematics

2.1.1 Kinematic model

The upper-limb kinematic chain consists of 7 DoFs (Degrees of Freedom) and 2 links, namely l_u for the upper arm and l_f for the forearm, respectively (Fig. 1). Three DoFs belong to the shoulder spherical joint; they are abduction–adduction q_1, flexion–extension q_2 and internal–external rotation q_3. The elbow revolute joint has 1 DoF that accounts for forearm flexion–extension q_4. Lastly, the wrist spherical joint is composed of pronation–supination q_5, ulnar-radial deviation q_6 and flexion–extension q_7 of the hand. Although the pronation–supination degree of freedom anatomically belongs to the elbow joint, it was considered as a wrist DoF, since it mainly affects hand orientation rather than its position.

In accordance with the Denavit–Hartenberg (D–H) convention [7], different frames were placed all along the upper-limb kinematic chain, starting from the reference frame (indicated as frame 0), placed in the shoulder joint. The frame locations, the D–H parameters, and the joint variables are described in Fig. 1a, b.

Given the D–H parameters, the homogeneous transformation matrix from frame i to the frame $(i-1)$, $T_i^{i-1}(q_i)$ is computed. Hence, the forward kinematics is given by $T_7^0(\bar{q})$ and describes the hand pose as a function of the joint angles vector $(\bar{q})$. Matrix $T_7^0(\bar{q})$ can be calculated as

$$\mathrm{T}_7^0(\bar{q}) = \mathrm{T}_3^0(q_1, q_2, q_3) * \quad \mathrm{T}_e(q_4) * \quad \mathrm{T}_7^4(q_5, q_6, q_7), \qquad (1)$$

where

i) $\mathrm{T}_3^0(q_1, q_2, q_3)$ accounts for translations and rotations of the elbow with respect to the reference frame;

ii) $\mathrm{T}_e(q_4) = \left[\mathrm{T}_4^3(q_4) \times \mathrm{Trans}(\hat{z}_4, l_f)\right]$, accounts for translations and rotations of the wrist with respect to the elbow frame;

iii) $\mathrm{T}_7^4(q_5, q_6, q_7)$, accounts for the rotations of the hand with respect to the wrist frame.

By regarding the human arm as redundant 7-DoFs manipulators [15], an additional variable can be introduced to describe the internal motion and exploit the kinematic redundancy. It is the *swivel angle* (α) as shown in Fig. 1d. It represents the angle between the reference plane, defined by vectors $\hat{V}$ and $s\bar{w}$ (Fig. 1—right side), and the plane containing $\bar{s} = O_0$, $\bar{e} = O_3$, $\bar{w} = O_7$, being O_i the origin of frame i. Therefore, the upper-limb internal motion can be described as a rotation of the plane containing arm joints around the vector $s\bar{w}$. Angle α is uniquely defined when shoulder and hand positions are fixed; in such a condition, the elbow can move along a circular arc (indicated as *internal motion*) having a normal vector aligned with vector $s\bar{w}$ [32].

2.1.2 Inverse kinematics algorithm with augmented Jacobian

The additional Cartesian variable expressed through swivel angle α allows solving the arm kinematic redundancy and, consequently, providing a closed-form solution for the inverse kinematics problem. In particular, the task space variables can be increased through the introduction of angle α in the hand pose vector as

$$\begin{bmatrix} \bar{m} \\ \alpha \end{bmatrix}, \qquad (2)$$

being $\bar{m}$ the (6×1) vector describing hand position and orientation.

Hence, the (6×1) velocity vector in the task space $(\bar{v})$ can be rewritten as a (7×1) vector given by

$$\begin{bmatrix} \bar{v} \\ \dot{\alpha} \end{bmatrix} \qquad (3)$$

and the corresponding square (7×7) *Augmented* Jacobian matrix is computed as

$$J_A(\bar{q}) = \begin{bmatrix} J_g(\bar{q}) \\ J_\alpha(\bar{q}) \end{bmatrix}. \qquad (4)$$

The augmented Jacobian is composed of two matrices; they are the geometric Jacobian matrix of the upper-limb $(J_g(\bar{q}))$, accounting for the contribution of the joint speed vectors to the hand velocity, and the swivel angle Jacobian $(J_\alpha(\bar{q}))$, i.e., a row vector that describes the contribution of the joint velocities to the rate of change of α. The computation of the swivel angle Jacobian is explained in detail in Sect. 2.2.1.

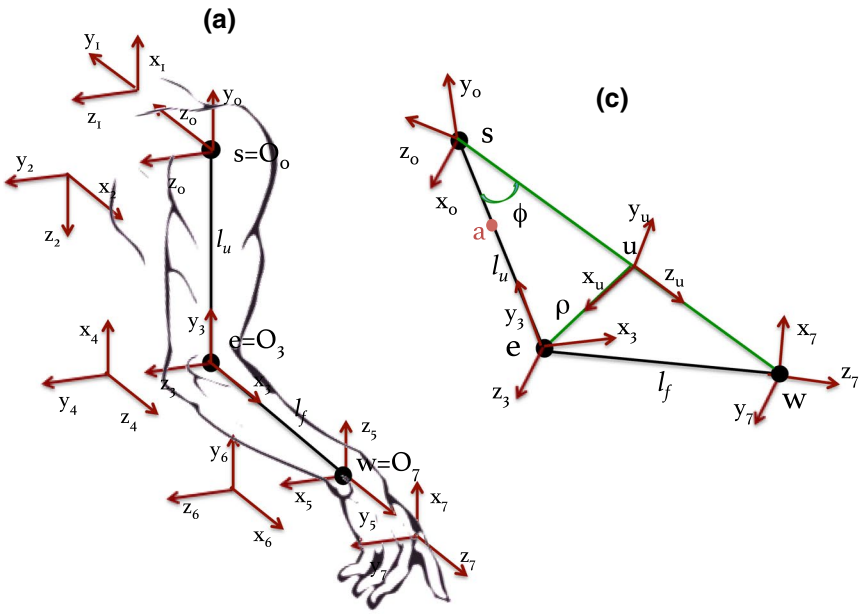

(b)

f_i	q_i	a_i	γ_i
0	π/2+q1	0	π/2
0	3π/2+q2	0	π/2
l_u	q3	0	−π/2
0	π/2+q4	0	π/2
0	π/2+q5	0	π/2
0	π/2+q6	0	π/2
0	π/2+q7	0	π/2

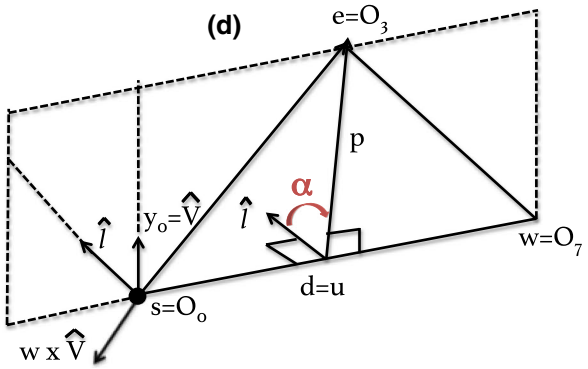

Fig. 1 **a** Upper-limb frames placement. **b** D–H parameters. **c** Representation of the variables needed for the computation of the elbow joint Cartesian coordinates. **d** Representation of the variables needed for the swivel angle computation

The inverse kinematics algorithm employing the augmented Jacobian matrix is expressed as

$$\dot{\bar{q}} = J_A^{-1}(\bar{q}) \left(\begin{bmatrix} \bar{v} \\ \dot{\alpha} \end{bmatrix} + K * \bar{er} \right). \tag{5}$$

Given hand velocity vector $\bar{v}$ and the rate of change of α , it allows computing joint speed vector $\dot{\bar{q}}$. The inversion error ($\bar{er}$), due to the time-discrete integration procedure for calculating joint trajectories ($\bar{q}$), can be reduced choosing a suitable value for gain matrix (K). In particular, as explained in [29], if K is a positive definite (usually diagonal) matrix, the system describing error time course is asymptotically stable and the inversion error tends to zero with a velocity of convergence proportional to the eigenvalues of K; however, being the inversion scheme implemented as a discrete-time system, an upper bound exists for the eigenvalues of K, depending on the sampling time.

Finally, in order to extend the algorithm also to regions closed to kinematic singularities, a damped least-squares augmented Jacobian matrix can be used in Eq. (5) in place of J_A. It can be expressed as

$$J_A^{\star} = J_A^T \left(J_A J_A^T + k^2 I \right)^{-1}, \tag{6}$$

where J_A^T represents the transpose augmented Jacobian matrix, k^2 is a damping factor useful for numerically conditioning the solution of the inverse kinematics procedure, and I is the (7×7) identity matrix. Damping factor k has to be positive definite and allows defining the weight between the minimum norm of the joint speed vector $||\dot{\bar{q}}||$ and the minimum inversion error. High values of k ensure limited joint speed and reduce accuracy in the neighborhoods of singularities; the appropriate choice of k depends on the minimum singular value of the Jacobian matrix,

since it represents a measure of proximity to singularities [30].

2.2 Joint reconstruction algorithm

The proposed method for upper-limb joint reconstruction was specifically conceived for being used during robot-aided therapy with end-effector machines. In this context, patient hand pose (and velocity) is provided by robot position sensors. Joint motion can be computed through the inverse kinematics algorithm in Eq. (5), once the augmented Jacobian matrix is calculated. Hence, the computation of the swivel angle and of the corresponding Jacobian vector $J_\alpha(\bar{q})$ is a key point. Both of them require the measuring elbow trajectory, as explained below.

2.2.1 Computation of the swivel angle

The swivel angle is the angle between the reference plane and the plane containing shoulder, elbow and wrist joints and is expressed as

$$\alpha = \text{atan2}\left(\hat{w}^T(\hat{V}\times\bar{p}), \hat{V}^T\bar{p}\right). \tag{7}$$

Note that the reference plane is not uniquely defined when vectors $\hat{V}$ and $s\bar{w}$ are colinear. Choosing $\hat{V}$ as a vertical unit vector, the alignment with $s\bar{w}$ is avoided if fully outstretch of the arm along the vertical axis is not permitted. The swivel angle can be computed as a function of elbow ($\bar{e}$) and hand ($\bar{w}$) positions, once defined the following three parameters (Fig. 1d):

- projection of $\bar{e}$ onto $\bar{w}$, indicated as $\hat{d} = \hat{w}(\hat{w}^T\bar{e})$,
- minimum distance between vector $s\bar{w}$ and the elbow joint, denoted with $\bar{p} = \bar{e} - \bar{d}$,
- vector lying on the reference plane and orthogonal to vector $s\bar{w}$, i.e., $\bar{l} = (\bar{w}\times\hat{V})\times\bar{w}$. The swivel angle Jacobian in Eq. (4) can be computed as

$$J_\alpha(\bar{q}) = \frac{\left(\hat{w}\times\hat{p}\right)^T}{||\bar{p}||}E + \left[\frac{\hat{V}^T\bar{w}}{||\bar{l}||}\left(\hat{w}\times\hat{l}\right)^T - \frac{\hat{w}^T\bar{e}}{||\bar{w}||\,||\bar{p}||}\left(\hat{w}\times\hat{p}\right)^T\right]W, \tag{8}$$

being

$$\dot{\alpha} = \frac{\left(\hat{w}\times\hat{p}\right)^T}{||\bar{p}||}\left[E - \frac{\hat{w}^T\bar{e}}{||\bar{w}||}W\right]\dot{\bar{q}} + \frac{\hat{V}^T\bar{w}}{||\bar{l}||}\left(\hat{w}\times\hat{l}\right)^T W\dot{\bar{q}} = J_\alpha(\bar{q})\dot{\bar{q}} \tag{9}$$

the time derivative of the swivel angle in Eq. (7) and E and W the Jacobian matrices that relate the joint speed vector to the translational velocities of elbow and wrist joints, respectively.

2.2.2 Computation of elbow joint trajectories

The method proposed in [21] was applied to determine the position of the elbow in the Cartesian space. To this purpose, an accelerometer placed on the upper arm was used to provide upper arm static acceleration. Hand position data provided by the robot and static acceleration provided by the accelerometer were used to estimate the vertical coordinate of the elbow joint e_y. It is worth observing that, thanks to the availability of hand kinematic data from robot position sensors, only one accelerometer was used (instead of a net of sensors) to reconstruct the entire arm kinematics; thus, the unobtrusiveness of the acquisition system was ensured. The remaining two Cartesian coordinates of the elbow joint were reconstructed by applying some geometrical considerations on arm internal motion.

The elbow joint Cartesian coordinates in the reference frame (shoulder frame) can be expressed as (Fig. 1c)

$$\bar{e} = \left[l_u\text{sin}q_1\text{cos}q_2 \;\; -l_u\text{cos}q_1\text{cos}q_2 \;\; -l_u\text{sin}q_2\right]^T. \tag{10}$$

The accelerometer placed in $\bar{\mathbf{a}}$ in Fig. 1 allows computing the elbow coordinate along y_0-axis as

$$e_y = \frac{-\ddot{a}_y l_u}{g} = -l_u\text{cos}q_1\text{cos}q_2, \tag{11}$$

where $\ddot{a}_y$ is the radial acceleration of the upper arm in $\bar{\mathbf{a}} = \left[a_x \;\; a_y \;\; a_z\right]^T$ (expressed in the elbow frame $O_3 - x_3, y_3, z_3$) and g represents the gravitational acceleration.

By analogy with the work in [21], it was chosen to locate the accelerometer directly on the segment connecting the shoulder and elbow joints in order to neglect distances a_x and a_z. Therefore, the measured acceleration is given by

$$\ddot{a}_y \approx g\text{cos}q_1\text{cos}q_2 + (l_u - a_y)\dot{q}_1^2\text{cos}q_2^2 + \dot{q}_2^2, \tag{12}$$

where $g\text{cos}q_1\text{cos}q_2$ represents the radial static acceleration of the upper arm, while $(l_u - a_y)\dot{q}_1^2\text{cos}q_2^2 + \dot{q}_2^2$ is the corresponding dynamic acceleration. Given the application to stroke rehabilitation, only slow upper-limb movements are considered; hence, in the recorded acceleration, the static component dominates on the dynamic term and dynamic acceleration can be neglected. Under this assumption, the radial acceleration measured on the upper arm is given by $\ddot{a}_y \approx g\text{cos}q_1\text{cos}q_2$.

On the other hand, to compute x and z components of the elbow position, a number of parameters need to be calculated. They are (Fig. 1c):

- The normal vector to the internal motion arc, i.e., $\hat{z}_u = \hat{w}$.
- The angle between vector $s\bar{w}$ and the upper arm segment; by invoking the cosine rule, it is expressed as

$$\phi = \text{acos}\frac{||s\bar{w} - \bar{s}||^2 + l_u^2 - l_f^2}{2l_u||s\bar{w} - \bar{s}||}.$$

- The radius and the center of the internal motion arc, given by $\rho = l_u \text{sin}\phi$ and $\bar{u} = l_u\hat{z}_u\text{cos}\phi$, respectively.
- The unit vectors $\hat{x}_u$ and $\hat{y}_u$ of the frame centered in $\bar{u}$. Unit vector $\hat{x}_u$ is determined as follows:

1. The vertical component of $\hat{x}_u$ is given by

$$\hat{x}_u^{(2)} = (e_y - u_y)/\rho;$$

2. The other two components of $\hat{x}_u$ can be computed through the system of equations

$$\begin{cases} ||\hat{x}_u||^2 = 1 \\ \hat{x}_u \cdot \hat{z}_u = 0. \end{cases}$$

This yields

$$x_u^{(1)} = \frac{\sqrt{x_u^{(2)^2} z_u^{(1)^2} z_u^{(2)^2} - \left(z_u^{(1)^2} + z_u^{(3)^2}\right)\left(x_u^{(2)^2}\left(z_u^{(2)^2} + z_u^{(3)^2}\right) - z_u^{(3)^2}\right)} - x_u^{(2)} z_u^{(1)} z_u^{(2)}}{z_u^{(1)^2} + z_u^{(3)^2}}$$

and

$$x_u^{(3)} = \frac{x_u^{(1)} z_u^{(1)} + x_u^{(2)} z_u^{(2)}}{z_u^{(3)}}.$$

3. Once computed $\hat{x}_u$ and $\hat{z}_u$, unit vector $\hat{y}_u$ is given in a right-handed frame.

- Finally, elbow position in the frame centered in $\bar{u}$. It is given by

$$\bar{e}_u = \begin{bmatrix} \rho & 0 & 0 \end{bmatrix}^T.$$

Hence, elbow coordinates in the reference frame can be calculated as

$$\begin{bmatrix} \bar{e} & 1 \end{bmatrix}^T = \mathbf{U} \begin{bmatrix} \bar{e}_u & 1 \end{bmatrix}^T, \tag{13}$$

being

$$\mathbf{U} = \begin{bmatrix} \hat{x}_u & \hat{y}_u & \hat{z}_u & \bar{u} \\ 0 & 0 & 0 & 1 \end{bmatrix} \tag{14}$$

the transformation matrix from the frame centered in $\bar{u}$ to the shoulder frame.

2.3 Experimental validation

The experimental validation has the twofold purpose of assessing method performance and evaluating method efficacy to discriminate pathological behavior during robot-aided motor tasks. Therefore, the following experimental activities were fulfilled:

1. A comparative analysis with joint angles obtained from an 8-camera marker-based optoelectronic motion capturing system (SMART-D, from BTS Bioengineering). It was carried out on healthy subjects and was aimed to compare joint angles trajectories and assess the performance of the proposed method the *root-mean-square error* (RMSE) and the maximum error of the reconstructed angles with respect to those computed through the motion analysis system were calculated.
2. The application to robot-aided rehabilitation, by reconstructing joint motion of healthy and stroke subjects performing circle-drawing tasks with a planar end-effector machine. It was applied to both patients and healthy subjects in order to evaluate the possibility to employ the presented method for discriminating healthy and stroke motion also in the joint space, a comparison between the reconstructed healthy and stroke subjects' motion was carried out.

All subjects gave informed consent to take part in this study that was approved by the local scientific and ethical committees.

2.3.1 Validation of the reconstruction algorithm: subjects and protocol

This testing phase was aimed at assessing the validity of the proposed method and measuring its performance by means of a comparative analysis with a marker-based optoelectronic measurement system. It involved four healthy subjects (two men and two women, mean age $= 27.6 \pm 1.9$ years).

Each subject was asked to seat on a chair, placing the hands on the thighs and the arms on the sides of the trunk; then, they were required to reach a target placed in front of them and return to the starting position (i.e., *forward/backward movements*) avoiding fast and jerky motion; each movement was repeated five times. The target, the same for all the tested subjects, was placed in front of the subject

and centered with respect to her/his chest so that it could be reached without fully out-stretching the elbow.

A wearable and light-weight magneto-inertial sensor (MTx sensors, from Xsens—full scale: $\pm 5g$) was positioned on the subject's upper arm; it is worth observing that, thanks to the availability of hand pose data from robot position sensors, only one magneto-inertial sensor was used (instead of a net of sensors) to reconstruct the entire arm kinematics; thus, the unobtrusiveness of the acquisition system was ensured. Since a triaxial accelerometer is embedded in the sensor, one of the sensor axes was aligned with the limb segment. Acceleration data were sampled at 200 Hz, sent to a computer via serial connection (RS-232) and offline filtered with a tenth-order Butterworth low-pass filter with a cutoff frequency of 100 Hz; filter order and cutoff frequency were selected through visual inspection of the acceleration signal, paying attention to remove only noise. Acceleration data were used to compute the swivel angle, once calculated the elbow trajectory [(Eqs. (7) and (13)]. Thus, the reconstruction algorithm was used to reconstruct arm joint angles. The input signals for the reconstruction algorithm in Eq. (5) were the hand pose, the lengths of upper arm and forearm segments and the shoulder position; they were provided by the optoelectronic system used for validating the method. The output data of the algorithm were the arm joint velocities; they were integrated through a numerical integration method (i.e., Euler's method), with a step-size of $0.005s$.

The optoelectronic system (Fig. 2a) was made of eight infrared digital cameras (sensors resolution 640×480 px, acquisition frequency 60–120 Hz), retro-reflective markers and one workstation for data processing and motion reconstruction; system accuracy is < 0.2 mm on a volume $4 \times 3 \times 3\,\mathrm{m}^3$. The system was used to measure the joint angles of the subject during the movements described above and compare them with the angles computed through the reconstruction algorithm. To this purpose, a kinematic protocol was developed in [24] and applied to the computation of the human arm angles. This protocol is a modified version of Rab protocol in [26]. Twelve retro-reflective markers were located on twelve arm anatomical landmarks, i.e., right and left acromion, 7th cervical vertebrae (C7), sternum, right/left olecranon, right/left distal ulna, right/left distal radius, 3rd metacarpus center of right/left hand, middle finger tip of right/left hand, right and left anterior superior iliac spine (ASIS) and sacrum. Then, the seven arm joint angles were computed starting from markers 3D coordinates [26] sampled at a frequency of 60 Hz and filtered through a sixth-order Butterworth low-pass filter with a cutoff frequency of 3 Hz [18]. Fig. 2b illustrates the experimental setup for the validation of the proposed method; in particular, it shows the subject red stick figure, plotted during recording, with retro-reflective markers (placed directly on subject skin) and the magneto-inertial sensor attached to the subject's upper arm.

Finally, in order to assess the performance of the proposed method in the reconstruction of the arm angles, the error (in terms of RMSE and maximum error) committed by the proposed method with respect to the measurements performed with the optoelectronic system was computed for all the joint trajectories in all the performed tests.

2.3.2 *Experimental trials of robot-aided rehabilitation: subjects and protocol*

Two chronic stroke patients (mean age 58.8 ± 1.2 years) were recruited for these experimental trials. They had a single stroke event more than 6 months before the enrollment in this study. A 18-session robot-aided treatment was delivered with a robotic machine for upper-limb training, i.e., the InMotion2 planar robot (Interactive Motion Technologies Inc.). Each subject was evaluated at admission to and discharge from

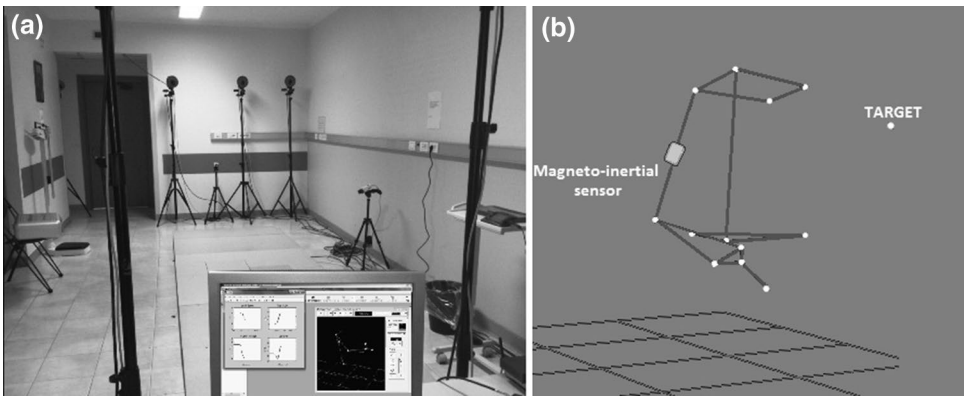

Fig. 2 **a** SMART-D BTS optoelectronic motion capturing system: post-processing of the experimental trails. **b** Experimental trial for assessing method validity: the placement of retro-reflective markers and magneto-inertial sensor is shown on the subject *stick* figure

Table 1 Patients data: lengths of upper arm and forearm segments—paretic arm—values of upper extremity FM-SE and MP-SE, before (PRE) and after (POST) the robotic treatment

Patient	Upper arm length (m)	Forearm length (m)	Paretic arm	Upper extremity FM-SE/42		Upper extremity MP-SE/70	
				PRE	POST	PRE	POST
1	0.35	0.32	Right	18	19	36	38
2	0.36	0.33	Left	18	21	42	43

this study through clinical scales (i.e., Fugl-Meyer [11] and Motor Power [23]) and quantitative measures provided by the joint motion reconstruction algorithm described in this paper. In particular, for the quantitative evaluation, patients were required to perform a series of unassisted circle-drawing exercises with the InMotion2 Shoulder–Elbow robot. Cartesian motion was monitored through position sensors embedded into the robot, and joint motion was reconstructed with the proposed algorithm in Eqs. (4), (5) and (6).

Table 1 reports data about the two enrolled patients. It reports the lengths of upper arm and forearm segments, in addition to the paretic arm (right or left) and the values of the Fugl-Meyer scale for shoulder–elbow (maximum score = 42 points), FM-SE/42, and the motor power scale for shoulder–elbow (maximum score = 70 points), MP-SE/70, at admission (i.e., PRE) and discharge (i.e., POST).

For comparative purpose, the same circle-drawing tasks were performed also by five healthy volunteers (age 26 ± 2.3 years) in order to define "healthy bands" for all the kinematic variables during the performed tasks.

The experimental trials were performed as follows. Healthy and stroke subjects were seated on a chair and required to perform five repetitions of a task consisting of drawing a counterclockwise circle in the horizontal plane starting at 3 o'clock. They were asked to move their hand along the desired circular trajectory (radius = 0.075 m) shown on a monitor in front of them, together with a visual feedback regarding the current hand position. The trunk of each subject was tied through a seat belt in order to avoid compensatory torso movements; the forearm was placed and secured through velcro straps on a plastic support attached to the robot end-effector in order to minimize forearm pronation–supination and wrist movements. Robot motors were turned off, and thus, no assistance was provided to subjects during the exercise. The hand position of each subject was provided by the sensors embedded into the robot (sampling frequency of 200 Hz). Moreover, the MTx sensor was placed on the subject's upper arm for the acquisition of the radial acceleration data; lengths of limb segments were manually measured.

In order to determine the shoulder position with respect to the robot base frame, an initial calibration phase was carried out. Hence, after measuring upper-limb segment lengths, the subject hand was positioned in the center of the circle (coincident with the robot workspace center) with a flexion angle of 45° for the shoulder and the elbow and an abduction angle of 45° for the shoulder; a goniometer was used for measuring calibration angles.

The circle-drawing task is a typical planar exercise for evaluating stroke patients after a robotic treatment [8]. In this study, it is particularly suitable to investigate the joint activity, mainly in the simultaneous activation of shoulder and elbow angles [8] that is typically compromised in stroke patients.

In Fig. 3a, a sketch of the top view of subjects' position while performing the circle-drawing task and robot reference system is illustrated; on the other hand, Fig. 3b shows one of the tested healthy subjects performing the task.

3 Results

3.1 Performance of the joint reconstruction algorithm

Figure 4 illustrates the mean data of the upper-limb joint reconstruction of the five *forward/backward movements* performed by one of the four tested subjects; in detail:

- the mean value of the seven arm angles reconstructed through Eq. (5) is drawn with a dotted black line, while the mean arm angles measured through the optoelectronic system are shown in light blue;
- the mean 3D hand trajectory obtained by applying the forward kinematics function to the seven reconstructed angles is shown with a dotted red line, while the mean hand position measured through the SMART-D optoelectronic system is drawn in blue;

- Additionally, Fig. 4 reports, in the lower part, the values of mean and maximum standard deviations in the computation of all the arm angles in the five *forward/backward movements* with the optoelectronic system (light blue rectangle) and with the proposed method (dotted black rectangle); mean and maximum standard deviations for the optoelectronic system are equal to 7.5×10^{-3} rad and 1.2×10^{-2} rad, while mean and maximum standard deviations for the proposed method are given by 2.3×10^{-2} rad and 3.7×10^{-2} rad.

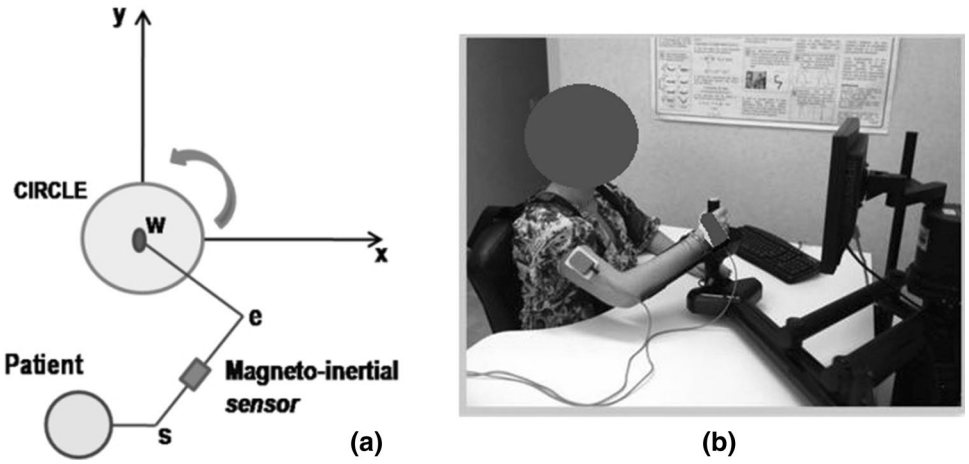

Fig. 3 Experimental trial of robot-aided rehabilitation: **a** a sketch of the *top view* of subjects' position while performing the *circle-drawing* task and robot reference system; **b** a healthy subject performing the *circle-drawing* task

In all the performed tests, the arm joint trajectories reconstructed with the proposed method are well overlapped with the angles computed through the optoelectronic motion capturing system, and the measures performed through the two systems have similar variability. The RMSE between the two trajectories in the joint space is 8.3×10^{-3} rad on average over all the performed experimental trials, with a variance of 1.8×10^{-3} rad^2.

A graphical representation of the error committed with the proposed reconstruction algorithm is shown in Fig. 5; it reports the RMSE (in gray) and the maximum error (in white) for each reconstructed upper-limb joint angle.

3.2 Experimental results of robot-aided rehabilitation

Figure 6 reports, in the upper part, the joint kinematic reconstructions of healthy and stroke subjects during the circle-drawing tasks performed with the InMotion2 robot. In particular, Fig. 6 shows the reconstructed shoulder angles q_1, q_2, q_3 in the top, elbow angle q_4 in the middle and the hand positions provided by the robot in the bottom. Wrist angles are not reported being negligible their variations during planar tasks with the InMotion2.

Healthy subjects' trajectories were reported as "healthy bands" (i.e., the standard deviations of the trajectories performed by the healthy volunteers), thus defining a reference behavior for evaluating patients' motion. Patients' trajectories are related to the phases of pre-treatment assessment (blue line) and post-treatment assessment (red line). They were averaged over all the five task repetitions and reported for both patients in two different columns.

As regards the variability of the showed data, the lower part of Fig. 6 reports mean and maximum standard deviations in joint and task spaces of the five task repetitions during PRE-treatment and POST-treatment for patient 1 (P1) and patient 2 (P2) and for the healthy subjects. Note that standard deviations decrease with motor recovery and are lower for healthy subjects, both in the joint and in the task space.

4 Discussion and conclusions

As detailed in Sect. 1, existent systems and methods for the reconstruction of the upper-limb kinematics (both analytical and geometrical) suffer from drawbacks that are difficult to cope with in robot-aided settings. As regards the commonly employed sensory systems for upper-limb motion capture, the major drawbacks are obtrusiveness, time-consuming initial calibrations, misalignment errors, necessity of highly structured environments; on the other hand, the major drawbacks of the existing computational methods are related to (1) the inconsistencies of the kinematic constraints used to solve the human upper-limb redundancy with some experimental observations, and (2) the inaccuracy in joint angles reconstruction due to the simplifications made in the geometrical approaches.

This work aims at overcoming the aforementioned limitations by proposing a novel method that allows reconstructing the 7-DoF upper-limb kinematics of the patients during robot-aided rehabilitation tasks in an unobtrusive and accurate way.

It is grounded on an analytical procedure of inverse kinematics borrowed from the robotic domain and based on the augmented Jacobian matrix. In particular, the issue of arm kinematic redundancy is solved through the augmentation of the task space and the definition of a new variable, i.e., the swivel angle of the arm; this allows obtaining a closed-form solution for the inverse kinematics problem. For the computation of the swivel angle, the coupled use of the rehabilitation robot with an accelerometer is proposed in order to record hand pose data with the robot and radial acceleration of the upper arm segment with the wearable sensor.

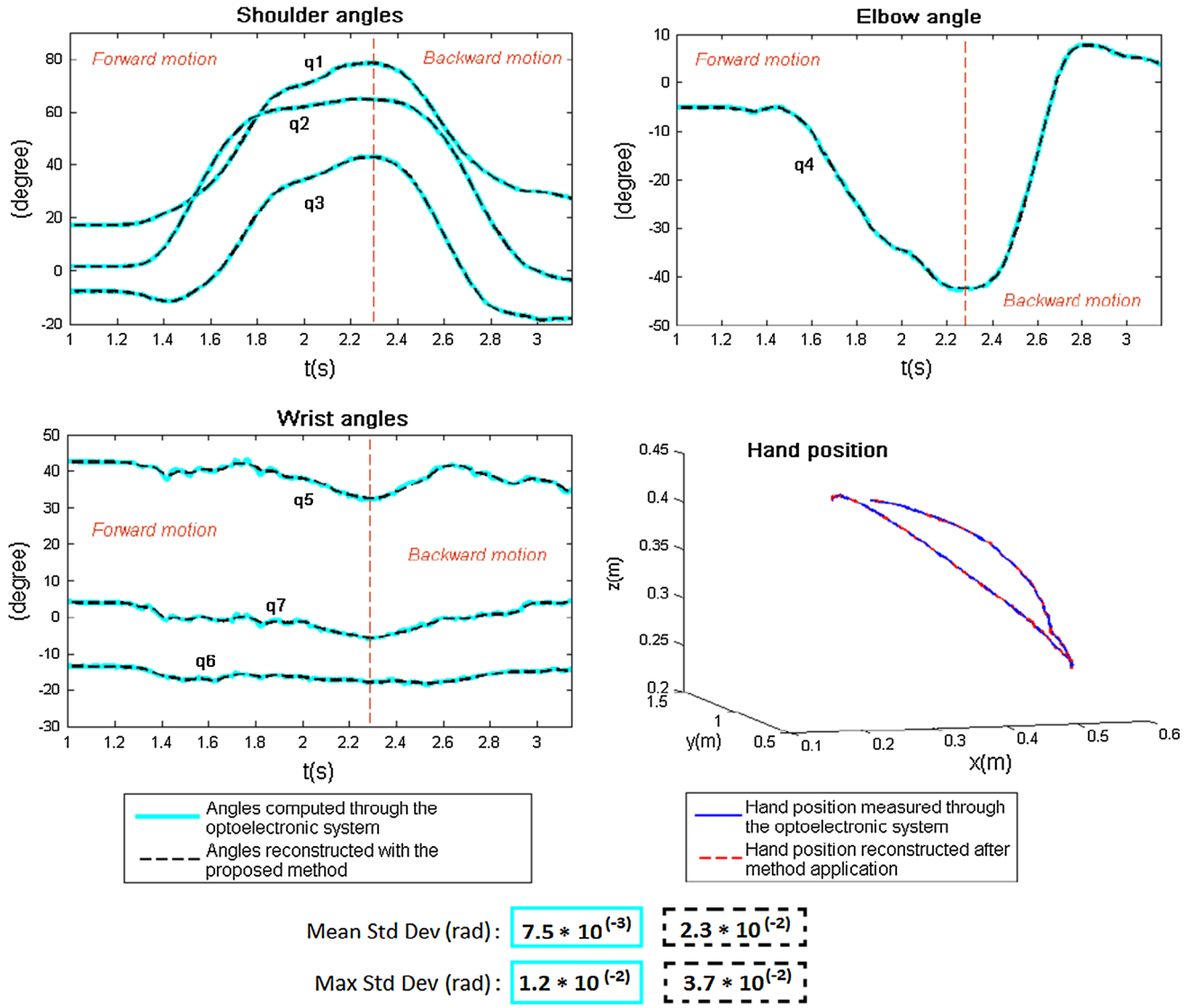

Fig. 4 Mean shoulder and elbow angles (in the *top*) and wrist angles (*lower left*) reconstructed with the proposed method (*dotted black line*) and measured through the optoelectronic system (*light blue line*). *Lower right* mean hand position computed by applying the arm forward kinematic function to the angles reconstructed with the proposed method (*dotted red line*) and measured through the optoelectronic system (*blue line*). *Bottom* mean and maximum standard deviations in the computation of all the arm angles in the five *forward/backward movements* with the optoelectronic system (*light blue rectangle*) and with the proposed method (*dotted black rectangle*)

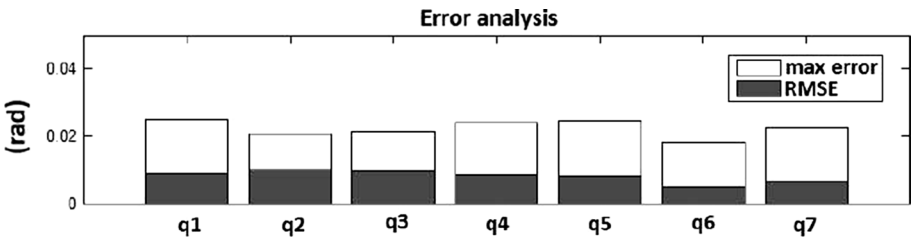

Fig. 5 RMSE (*gray*) and maximum error (*white*) between joint angles computed with the proposed method and obtained via the optoelectronic system

A detailed description of the arm kinematics and the theoretical formulation of the inverse kinematics algorithm have been firstly described in this paper. Subsequently, the experimental validation has been presented. It consisted of two main sessions: The first has measured method accuracy through the comparison with a marker-based optoelectronic system; the second one has provided an evidence of the applicability of the method to robot-aided rehabilitation

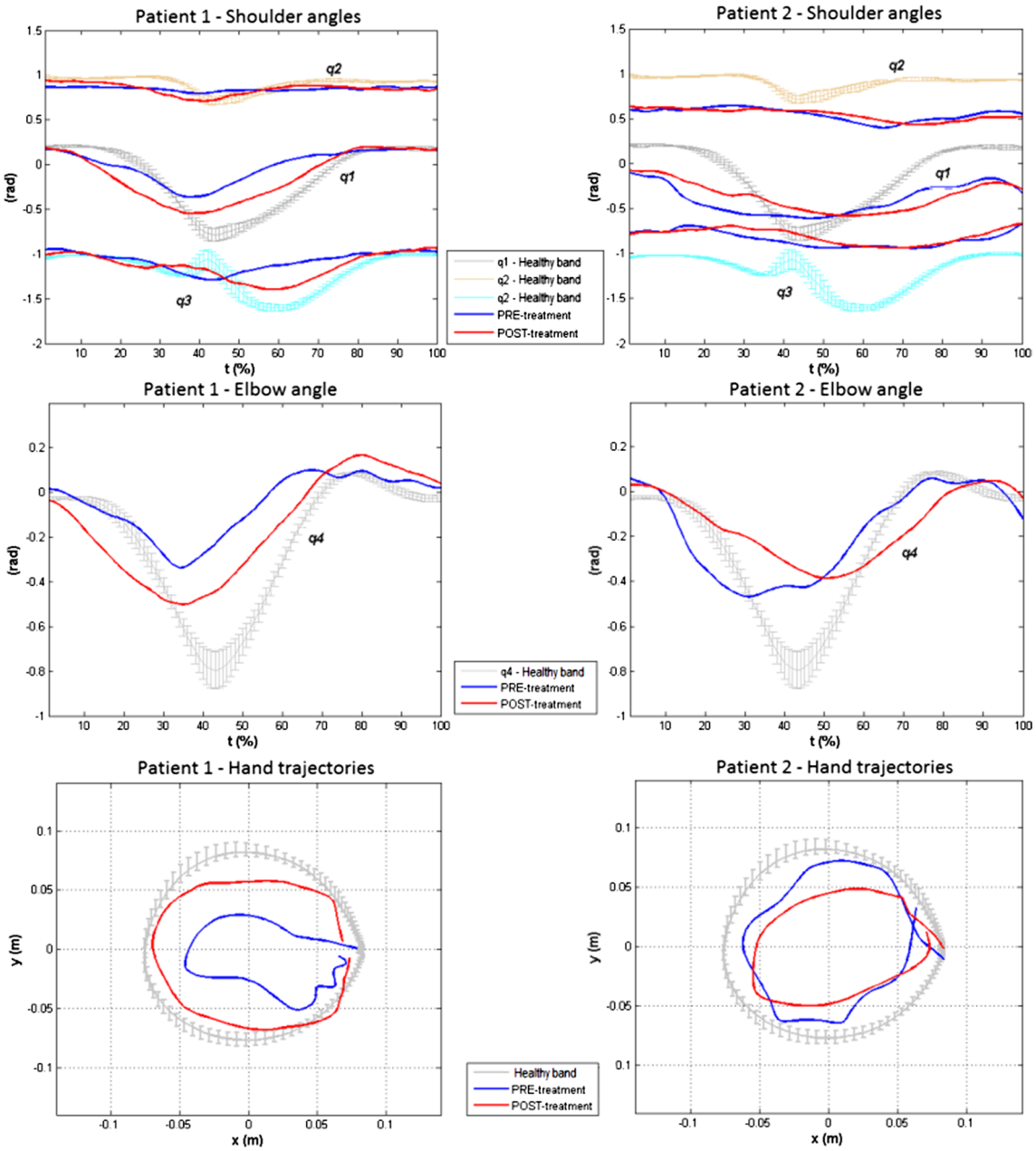

	Joint space data variability				*Task space data variability*			
	PRE-treatment		**POST-treatment**		**PRE-treatment**		**POST-treatment**	
	Mean Std Dev (rad)	**Max Std Dev (rad)**	**Mean Std Dev (rad)**	**Max Std Dev (rad)**	**Mean Std Dev (m)**	**Max Std Dev (m)**	**Mean Std Dev (m)**	**Max Std Dev (m)**
P1	0.3714	0.7123	0.2987	0.5531	0.059	0.091	0.042	0.073
P2	0.4923	0.8919	0.3176	0.6917	0.07	0.105	0.063	0.08
	Healthy subjects				**Healthy subjects**			
	Mean Std Dev (rad)		**Max Std Dev (rad)**		**Mean Std Dev (m)**		**Max Std Dev (m)**	
	0.0871		0.160		0.008		0.014	

Fig. 6 *Top* shoulder and elbow angles and hand trajectories of healthy and stroke subjects. Healthy subjects trajectories are depicted as "healthy bands"; stroke patients' data are averaged over all the five task repetitions. *Blue* pre-treatment; *red* post-treatment. *Bottom* mean and maximum standard deviations of the showed data both in joint and in task space

for patient assessment, with preliminary results on stroke patients.

As regards method accuracy, the algorithm has revealed good results in reconstructing all the arm angles with a RMSE error of 8.3×10^{-3} rad (and variance of 1.8×10^{-3} rad) with respect to the measures performed with a commercial optoelectronic motion capturing system. Interestingly, our analysis has also shown that the angles measured through the two systems have similar variability.

Also the error evolution over time of the inverse kinematics algorithm in Eq. (5) was analyzed. In the upper part of Fig. 7, the norm of the error [(i.e., variable $\bar{er}$ in Eq. (5)] during the inverse kinematics procedure with the augmented Jacobian is showed; in particular, the norm of position error, orientation error and swivel angle error are reported with an initial condition of $\bar{q} = [0.43, -0.1, -0.7, -0.7, 0.68, -0.56, -0.14]^T$ rad (i.e., the initial value of the joint angles measured through the optoelectronic system) for the arm joint vector, a gain matrix of $K = diag\{10 \ldots 10\}$ N/ms and a damping factor of $k^2 = 0.5$ (both chosen through a "trial and error" approach). As expected, although the error increases at the beginning, it rapidly converges to zero during movement reconstruction. In the lower part, Fig. 7 shows the desired task space variables (blue line), given as input to the proposed inverse kinematics method, and the task space trajectories obtained by method application (red line).

The error between the two methods (even though it is low) can be due to a number of reasons: e.g., subtle and unavoidable trunk movements that entail small displacements of the reference frame, markers movements on the skin during the task execution, which can produce a small error in the measure of the length of the upper-limb segments (however, in the absence of an optoelectronic system, manual measurements of these lengths could be even more inaccurate), the neglected dynamic component of the acceleration that is presumably low but not null. Neglecting dynamic component of acceleration is not so limiting for the application of the method to robot-aided settings where patient motion is typically slow. However, it is worth noticing that the method cannot provide accurate results when the upper-limb is fully outstretched (elbow joint completely extended); hence, this configuration should be avoided.

On the other hand, in comparison with other methods in the literature, one can observe that: (1) the computational methods based on intrinsic kinematic constraints were found, in some cases, inconsistent with the experimental observations [19]; no inconsistencies were observed for the proposed method with the experimental analysis; (2) the accuracy of the proposed method for slow motions is higher than accuracy of methods based on geometrical approaches [21]; in fact, thanks to the exploitation of a sophisticated analytical procedure, the maximum RMSE in

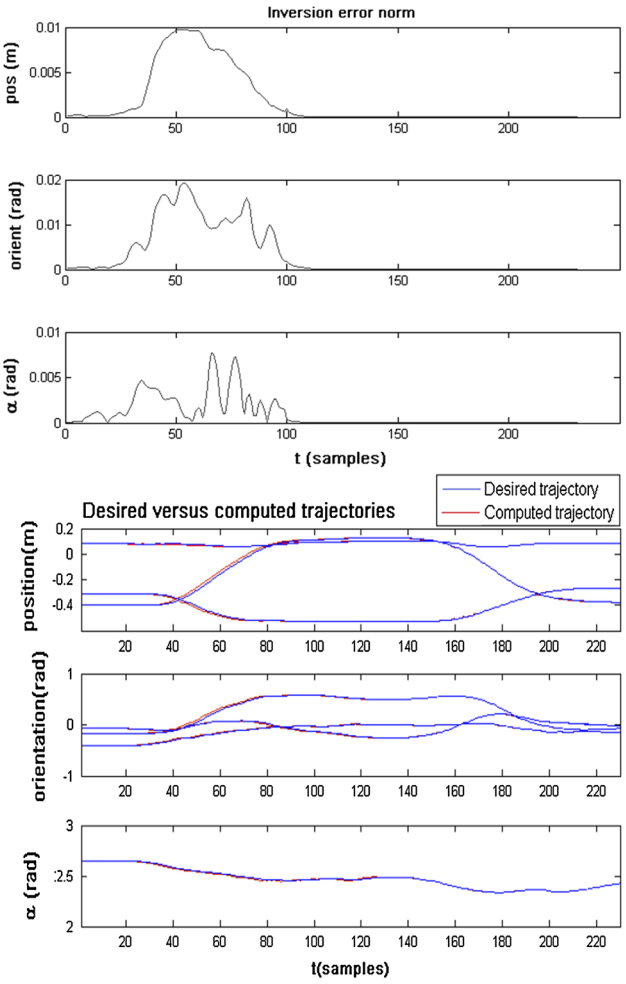

Fig. 7 *Top* norm of the error $\bar{er}$ due to the time-discrete integration; the error relative to position variables (*above*), orientation variables (*middle*) and swivel angle (*below*) during the reconstruction of a *forward/backward movement* is represented. *Bottom* representation of task space desired trajectories (*blue line*) and task space trajectories computed through the inverse kinematics procedure (*red line*)

the computation of arm angles with the proposed method is equal to 2.7×10^{-2} rad, while in [21] it is greater than 5×10^{-2}rad.

As regards the application to robot-aided rehabilitation, five healthy subjects and two patients were evaluated with the proposed method while performing a circle-drawing task with the InMotion2 planar robot. The reported plots on the mean value of the reconstructed data have shown a clear difference between healthy and pathological behavior. Motion variability was assessed with the standard deviations of the reconstructed kinematic data; they decrease with motor recovery and are lower in the case of healthy motions, both in joint and in task space.

Moreover, it clearly emerges from Fig. 6 that hand trajectories close to those of healthy subjects are obtained

with joint trajectories that tend to the "healthy bands" of the angles. This finding seems to be in line with the results on stroke patients in [8]; in it, although the joint trajectories were related to a simplified 2-DoF model of the upper-limb, it was observed that during motor recovery from stroke the improvement in drawing circles is accompanied by the increase in the excursion of the shoulder and elbow angles.

It is also worth observing that the outcomes for the two tested patients in Fig. 6 are different: performance of patient 1 in drawing the circle at the end of the treatment is higher than patient 2. This result seems to be controversial with the clinical scales reported in Table 1, since at the discharge patient 2 has higher clinical scores than patient 1. However, an in-depth analysis of all the items of the clinical scales revealed that the score of patient 2 was due to the improvement of 2 points on the FM scale for forearm pronation–supination. This is a DoF that is not exploited during the planar evaluation task performed with the InMotion2 robot; thus, its improvement does not contribute to circle drawing. However, also consider that this work wants basically to assess method feasibility. The reconstruction of the upper-limb kinematics during robot-aided tasks with end-effector machines has pointed out the capability of identifying from patients' plots movement features in the joint space that are responsible for hand motion far from the "healthy bands." In particular:

- The coordination of shoulder and elbow joints during circle-drawing tasks is a key point since such a correlation in the paretic arm of stroke patients changes with robotic therapy [8]; in Fig. 6a, different degree of correlation between shoulder and elbow joints can be observed in the two patients that show also a different recovery level.
- The difficulty of patients to draw large circles can be due to their inability to properly extend the elbow joint; as described in [4], the pathological flexor synergy, occurring in same stroke patients, consists of elbow flexion combined with shoulder abduction and flexion.
- The meager movement smoothness in the Cartesian space can originate from a low smoothness in the joint space; it is widely recognized that movement smoothness improves during motor recovery [9].

- The reconstruction of arm joint trajectories of stroke patients undergoing robot-aided therapy has many practical implications that will be exploited in future work. In particular, through the definition of suitable indicators describing the kinematic performance of the patient in the joint space, a more exhaustive quantification (with respect to the sole use of hand position data) of patient residual motor capabilities will be possible. This is expected to provide, on one hand, a thorough evaluation of the outcomes of the therapeutic approach and, on the other hand, an objective basis for re-planning and/or tailoring the robotic treatment based on patient needs.

Future studies will be addressed to account for a larger number of subjects and for other tasks, such as 3D exercises or Activities of Daily Living, that also include wrist motion. Finally, an in-depth understanding of pathology-related motor strategies as well as the identification of stroke-specific movement features could be achieved.

Acknowledgments This work was partly supported by the European project H2020/AIDE (CUP J42I15000030006) and the Italian project Industria2015/DAHMS (CUP B85E10003020008).

References

1. Badler N, Tolani D (1996) Real-time inverse kinematics of the human arm. Presence 5:393–401
2. Balasubramanian S, Colombo R, Sterpi I, Sanguineti V, Burdet E (2012) Robotic assessment of upper limb motor function after stroke. Am J Phys Med Rehabil 91:S255–S269
3. Bosecker C, Dipietro L, Volpe BT, Krebs HI (2010) Kinematic robot-based evaluation scales and clinical counterparts to measure upper limb motor performance in patients with chronic stroke. Neurorehabil Neural Repair 24:62–69
4. Cirstea MC, Levin MF (2000) Compensatory strategies for reaching in stroke. Brain 123:940–953
5. Colombo R, Pisano F, Micera S et al (2008) Assessing mechanisms of recovery during robot-aided neurorehabilitation of the upper limb. Neurorehabil Neural Repair 22:50–63
6. Colombo R, Sterpi I, Mazzone A, Pisano F, Delconte C (2011) Modeling upper limb clinical scales by robot-measured performance parameters. In: IEEE international conference on rehabilitation robotics (ICORR) (pp 1–5)
7. Denavit J, Hartenberg SH (1955) A kinematic notation for lower-pair mechanisms based on matrices. ASME J Appl Mech 22:215–221
8. Dipietro L, Krebs HI, Fasoli SE, Volpe BT, Stein J, Bever C, Hogan N (2007) Changing motor synergies in chronic stroke. J Neurophys 98:757–768
9. Dipietro L, Krebs HI, Fasoli SE, Volpe BT, Hogan N (2009) Submovement changes characterize generalization of motor recovery after stroke. Cortex 45:318–324
10. Flash T, Meirovitch Y, Barliya A (2012) Models of human movement: trajectory planning and inverse kinematics studies. Rob Auton Syst 61:330–339
11. Fugl-Meyer AR, Jaasko L, Leyman I, Olsson S, Steglind S (1975) The post stroke hemiplegic patient. A method for evaluation of physical performance. Scand J Rehabil Med 7:1331
12. Go AS, Mozaffarian D, Roger VL (2013) Heart disease and stroke statistics—2013 update : a report from the American heart association. Circulation 127:e6–e245
13. Guglielmelli E, Johnson MJ, Shibata T (2009) Guest editorial special issue on rehabilitation robotics. IEEE TRO 25:477–480
14. Kim H, Miller LM, Byl N, Abrams G, Rosen J (2012) Redundancy resolution of the human arm and an upper limb exoskeleton. IEEE Trans Biomed Eng 59:1770–1779
15. Kreutz-Delgado K, Long M, Seraji H (1990) Kinematic analysis of 7 DoF anthropomorphic limb. Proc IEEE Int Conf Robot Autom 2:824–830

16. Langhorne P, Bernhardt J, Kwakkel G (2011) Stroke rehabilitation. Lancet 377:1693–1702 (review. Neurorehabil Neural Repair. 22:111121)
17. Li Z, Kim H, Milutinovi D, Rosen J (2013) Synthesizing redundancy resolution criteria of the human arm posture in reaching movements. In: Milutinovi D, Rosen J (eds) Redundancy in robot manipulators and multi-robot systems. Springer, Berlin, pp 201–240
18. Mayagoitia Ruth E, Nene Anand V, Veltink Peter H (2002) Accelerometer and rate gyroscope measurement of kinematics: an inexpensive alternative to optical motion analysis systems. J Biomech 35(4):537–542
19. Medendorp WP, Crawford JD, Henriques DYP, Van Gisbergen JAM, Gielen CCAM (2000) Kinematic strategies for upper arm-forearm coordination in three dimensions. J Neurophys 84:2302–2316
20. Mehrholz J, Hdrich A, Platz T, Kugler J, Pohl M (2012) Electromechanical and robot-assisted arm training after stroke updated review. Stroke 43(12):e172–e173
21. Mihelj M (2006) Hum Arm Kinemat Robot Based Rehabil. Robotica 24:377–383
22. Norouzi-Gheidari N, Archambault PS, Fung J (2012) Effects of robot-assisted therapy on stroke rehabilitation in upper limbs: systematic review and meta-analysis of the literature. J Rehabil Res Dev 49:479–496
23. OBrien MD (1986) Aids to the examination of the peripheral nervous system (3rd edn). London. Bailliere Tindall
24. Papaleo E, Zollo L, Sterzi S, Guglielmelli E (2012) An inverse kinematics algorithm for upper-limb joint reconstruction during robot-aided motor therapy. In: BIOROB-IEEE/RAS-EMBS international conference on biomedical robotics and biomechatronics (pp 1983–1988)
25. Patel S, Park H, Bonato P, Chan L, Rodgers M (2012) A review of wearable sensors and systems with application in rehabilitation. J Neuroeng Rehabil 9:1–17
26. Rab G, Petuskey K, Bagley A (2002) A method for determination of upper extremity kinematics. Gait posture 15(2):113–119
27. Richards L, Pohl P (1999) Therapeutic interventions to improve upper extremity recovery and function. Clin Geriatr Med 15:819–832
28. Rohrer B, Fasoli S, Krebs HI et al (2002) Movement smoothness changes during stroke recovery. J Neurosci 22:8297–8304
29. Sciavicco L, Villani L (2009) Robotics: modelling, planning and control. Springer, Berlin
30. Siciliano B (1990) Kinematic control of redundant robot manipulators: a tutorial. J Intell Robot Syst 3(3):201–212
31. Soechting JF, Buneo CA, Herrmann U, Flanders M (1995) Moving effortlessly in three dimensions: Does donders law apply to arm movement? J Neurosci 15:6271–6280
32. Tolani D, Goswami A, Badler NI (2000) Realtime inverse kinematics techniques for anthropomorphic limbs. Graph Models 62:353–388